ACS APPLIED MATERIALS & INTERFACES

Research Article

www.acsami.org

Long-Term Cycling Studies on Electrospun Carbon Nanofibers as Anode Material for Lithium Ion Batteries

Yongzhi Wu,[†,‡,§] M.V. Reddy,*[,‡] B. V. R. Chowdari,[‡] and S. Ramakrishna[§]

[†]NUS Graduate School for Integrative Sciences and Engineering, National University of Singapore (NUS), Singapore 119260

[‡]Department of Physics, National University of Singapore, Singapore 117542

[§]Department of Mechanical Engineering, Center for Nanofibers & Nanotechnology, NUS Nanoscience and Nanotechnology Initiative, NUS, Singapore 117581

Supporting Information

ABSTRACT: Electrospun carbon nanofibers (CNF) have been prepared at different calcination temperatures for a prolonged time (12 h) derived from electrospun polyacrylonitrile (PAN) membranes. They are studied as anode materials in lithium ion batteries due to their high reversible capacity, improved long-term cycle performance, and good rate capacity. The fibrous morphologies of fresh electrodes and tested samples for more than 550 cycles have been compared; cyclic voltammogram (CV) has also been studied to understand the lithium intercalation/deintercalation mechanism of 1D nanomaterials. CNFs demonstrate interesting galvanostatic performance with fading capacity after the first few cycles, and the capacity increases during long-term cycling. The increasing capacity is observed accompanied by volumetric expansion on the nanofibers' edge. Results of rate capacity have also been explored for all CNF samples, and their stable electrochemical performances are further analyzed by the galvanostatic intermittent titration technique (GITT) and electrochemical impedance spectroscopy (EIS). CNF carbonized at 800 °C is found to have a larger lithium ion storage ability and better cyclic stability than that carbonized at 600 and 1000 °C.

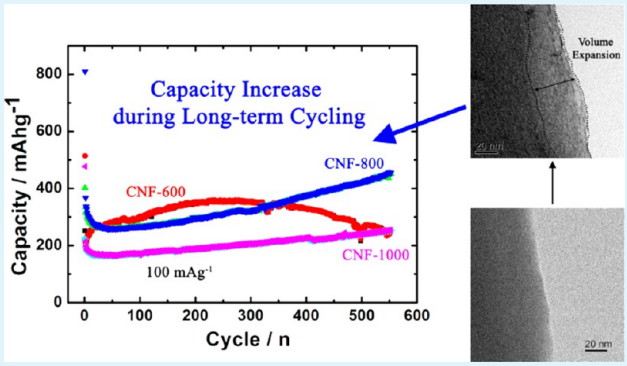

KEYWORDS: *electrospun CNF, long-term cycling, lithium ion battery, anode material*

INTRODUCTION

In recent years, the lithium ion battery (LIB) has arisen with the advancing technology of portable electronics (digital cameras, mobile phones, ipads, and so forth)[1−4] and has been extensively studied due to its wide application from delicate medical devices[5] to large electric vehicles. To achieve high energy and power density in demand, novel materials and nanostructures are explored for LIB electrode materials, in which anode materials play a significant role. The anode material reaction mechanisms are classified into four different mechanisms.[4] Commercial graphite anodes undergo an intercalation mechanism during cycling. With a similar reaction mechanism for titanium oxides[6−8] and lithium titanium oxides,[9,10] they can withstand a high rate of Li intercalation−deintercalation, thus exhibiting high power capability; yet, they suffer from limited capacity, namely, ∼150 $mAhg^{-1}$, much less than the theoretical reversible capacity of graphite, 372 $mAhg^{-1}$. Tin oxide (SnO_2) and Silicon (Si) remain as other favorable alternatives, providing high capacity, from 1130 to ∼3500 $mAhg^{-1}$, and stable performance when they are carefully designed into 1D nanostructures.[11−13] However, they still suffer from large irreversible capacity loss during the initial discharge, capacity fading during long-term cycling, and insufficient electronic conductivity. Furthermore, in comparison with carbonaceous materials, especially commercial graphite, cost stands as another issue. Therefore, it is still of great importance to find cost-effective, sustainable anode materials for the next generation of LIB aimed at both high energy and power density.

The carbon nanofiber (CNF) is an interesting candidate among carbonaceous anode materials due to its 1D nanostructure, good electronic conductivity, and free-standing characteristeristics.[14−18] The 1D nanostructure of CNF can be utilized to accommodate other electro-active materials, mitigating their own drawbacks and compensating for the electronic conductivity of the whole composite.[14] The appearance of CNF can be made into free-standing electrodes without use of any binders or conductive additives, by using the electrospinning technique.[16] Such procedures not only cut the cost of binders and conductive additives but also make the electrodes of pure carbonaceous material. Providing that the free-standing CNFs which are designed have robust body and

Received: September 26, 2013
Accepted: October 30, 2013
Published: October 30, 2013

sufficient conductivity, it is also possible to even abandon the current collector, copper foil, further reducing the price of electrode fabrication. Apart from bare CNFs, other derivative morphology (hollow CNFs[19]) or compositions (N-doped porous CNFs[20]) have been studied to demonstrate superior anodic properties, especially their capability of high power.

The electrospinning technique is a well-known nanotechnology capable of tailoring nanofibers of high ratio aspect ~10 000 on a large scale with versatility and a straightforward process.[21−23] Poly(acrylonitrile) (PAN) is the most favorable CNF precursor due to its high yielding rate of ≈50% and industry maturity of producing carbon fibers.[14,24,25] Interestingly, this thermoplastic polymer does not melt easily but is oxidized in air at high temperatures (> 230 °C), maintaining its original shape and readiness for carbonization.[26] It can be easily electrospun into nanofiber membranes carrying other metal salts so that it is also facile to fabricate CNF−metal oxide nanocomposites. Zhang and co-workers have thoroughly explored various electrode materials incorporated with CNFs using electrospinning.[17,27,28] The nanocomposites reported previously can generally sustain large current-rate cycling delivering higher reversible capacity; however, their long-term cycling ability has rarely been investigated to understand the very mechanism of Li intercalation/deintercalation and the capability of real application for such 1D nanostructure CNFs. Also, there are no studies on the electrochemical analysis of electrospun CNFs prepared at low carbonization temperature, where their conductivity largely depends upon pyrolysis temperature and time.[29] In this study, bare electrospun CNFs were prepared using an electrospinning polymeric solution of PAN and subsequent thermal treatment for a prolonged time (12 h). Their microstructures were compared before and after electrode discharge−charge for 550 cycles, and the electrochemical performances of CNFs were also investigated as a function of carbonization temperature.

EXPERIMENTAL SECTION

PAN (M_w ~150 000, 99%) and *N*, *N*-dimethylformamide (DMF, 99%) were purchased and used as received from Sigma-Aldrich.

One gram of PAN was added into 12.5 mL of DMF to form a homogeneous and transparent polymeric solution after it was vigorously stirred for 3 h. The electrospinning process was then carried out with a high voltage (17 KV) linked to the needle tip of a syringe offering the well-prepared solution at a flow rate of 0.8 mL h^{-1}. A white, ultrafine membrane consisting of nanofibers could be collected on the alumina foil 12 cm away from the needle tip. The fibrous mat was further dried in the oven at 60 °C to evaporate all DMF solvent.

The as-prepared electrospun nanofibers were first stabilized in an ambient pressure at 280 °C for 2 h at a ramping rate of 5 °C min^{-1} and then carbonized at 600, 800, and 1000 °C for 12 h under the protection of argon atmosphere, respectively. The corresponding products obtained were noted as CNF-600, CNF-800, and CNF-1000, respectively.

As is typical for electrochemical studies,[30,31] the electrospun CNF was milled and mixed with super carbon black and binder (polyvinylidene difluoride, PVDF) in the weight ratio of 70:15:15 using *N*-methyl pyrrolidinone (NMP) as dissolving solvent. The mixture was stirred overnight to form homogeneous slurry, which was further spread on an etched copper foil (thickness, 15 μm, Alpha Industries Co. Ltd., Japan) as current collector by using a doctor-blade technique. The copper foil was then dried at 80 °C under vacuum and cut into circular disks (16 mm in diameter) to serve as testing electrodes. Lithium metal foil (Kyokuto metal Co., Japan) as a counter electrode, 1 M $LiPF_6$ in ethylene carbonate (EC), diethyl carbonate (DEC) (1:1 in volume) (Merck) as an electrolyte, and Celgard 2502 membrane as separator were assembled together with testing electrodes to obtain 2016-type coin cells in an argon-filled glove box (MBRAUN, Germany). Before all electrochemical measurements, cells were aged for 12 h and then tested for cyclic voltammetry (CV) measurement, charge-discharge cycling, GITT, and EIS studies; they were performed between 0.005 and 3 V versus Li/Li^+ using a computer controlled by an Arbin Battery tester (U.S.A.). Rate capacity studies were also conducted ranging from 0.1 to 1 Ag^{-1}. EIS was measured on the cell with a Solartron impedance/gain-phase analyzer (model SI 1255) coupled with a potentiostat (SI 1268) at room temperature. The frequency ranged from 0.18 to 2 mHz with an ac signal amplitude of 10 mV. The impedance data were analyzed using Z-view software (version 2.2, Scribner Assoc., Inc., U.S.A.).

The morphological appearance and size of the as-prepared CNFs and long-term cycled CNFs (obtained by opening cells, dipping electrodes in propylene carbonate (PC) solution and further drying) were observed using a JEOL JSM-6700F scanning electron microscope (SEM). For each sample, at least 50 readings for the nanofiber diameters were recorded to make the histogram. Raman spectroscopy and X-ray diffraction (XRD, Xpert MPD PANalytical) were employed to characterize the carbonized structures of electrospun CNFs. The specific surface area and porosity of CNFs were retrieved using nitrogen adsorption at 77K using the Brunauer−Emmett−Teller (BET) measurement by Micromeritics (Tristar 3000, U.S.A.). The differences between fresh CNF-800 and long-term cycled electrodes were also investigated by a high-resolution transmission electron microscope (HR-TEM, JEOL-JEM 3010).

RESULTS AND DISCUSSION

Morphology and Characterization. Figure 1a−c show the SEM images of composite fresh electrodes made of carbon black, PVDF, and CNF, corresponding to CNF-600, CNF-800, and CNF-1000, respectively. The histograms in the insets demonstrate the distribution of fiber diameter before Li cycling. CNF carbonized at 600 °C has a wider range of diameter ranging from 210 to 370 nm with an average value of 310 nm, while CNF-800 (170−270 nm in range; average: 210 nm) and CNF-1000 (160−260 nm in range; average: 200 nm) exhibit similar diameter values. The result is consistent with the significant weight loss and structure change for PAN-derived carbon fibers carbonized at temperature higher than 700 °C.[32,33] This result can also be confirmed by the carbon yielding rate for different electrospun CNFs, which is the ratio of the weight of as-obtained CNFs to that of oxidized PAN nanofibers: the value for CNF-600, CNF-800, and CNF-1000 is 64.8, 15.2, and 4.7%, respectively. Similar to carbon fibers,[34,35] the dramatic weight loss of PAN nanofibers is possibly attributed to the removal of non-carbon (nitrogen, hydrogen, and oxygen) elements during the prolonged calcination time up to 12 h, when CNFs finally turned out to be thermo-stable, thus leading to the smaller diameter of electrospun nanofibers. The similarity of nanofiber diameter for CNF-800 and CNF-1000 is due to the relatively small variation of their carbon yielding rates. This indicates that the increase of carbonization

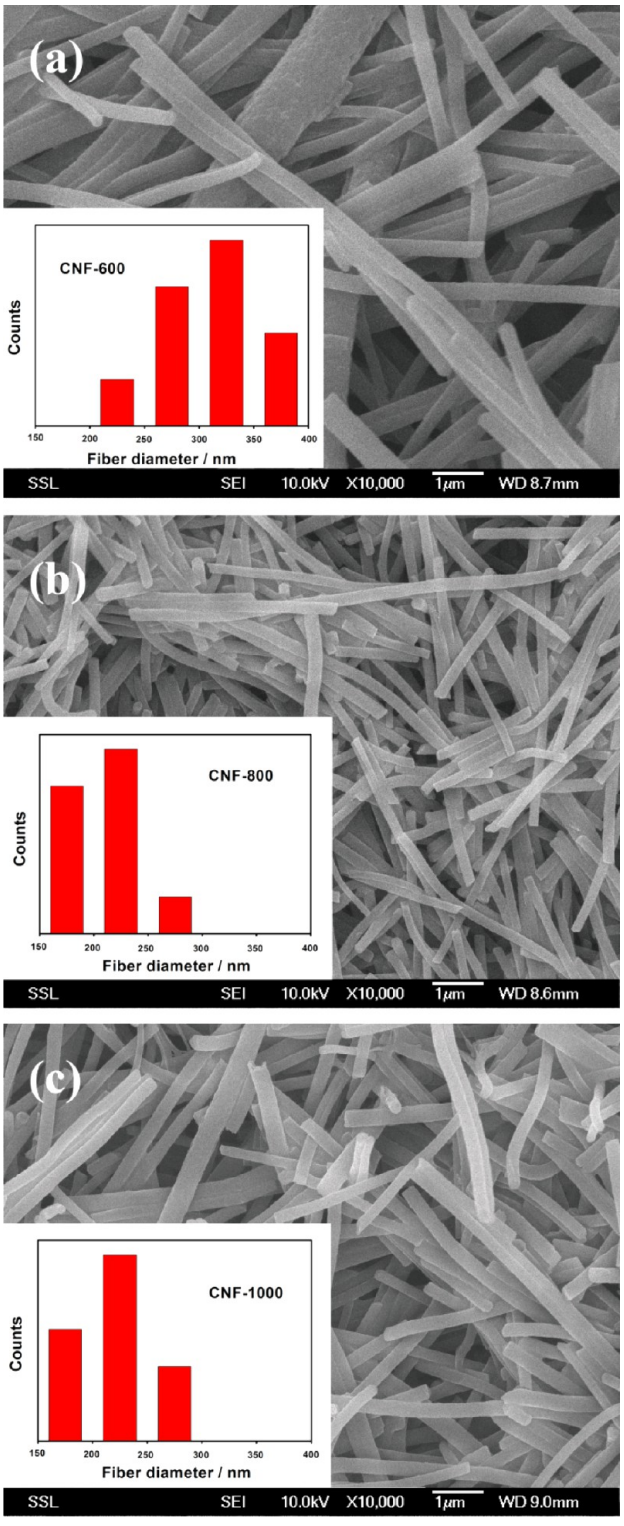

Figure 1. SEM images of fresh electrodes with histograms of fibrous diameter. (a) for CNF-600, (b) for CNF-800, and (c) for CNF-1000.

temperature higher than 800 °C would not change CNFs' diameter to a large extent. The long-time calcination is preferred to enhance the electronic conductivity of electrospun CNFs according to a previous study.[29]

Electrospun CNFs prepared under different conditions were also characterized using XRD, Raman spectroscopy, and BET measurement. In Figure 2a, XRD patterns clearly demonstrate the primary peak for the graphitic layers at 2θ around 25°,

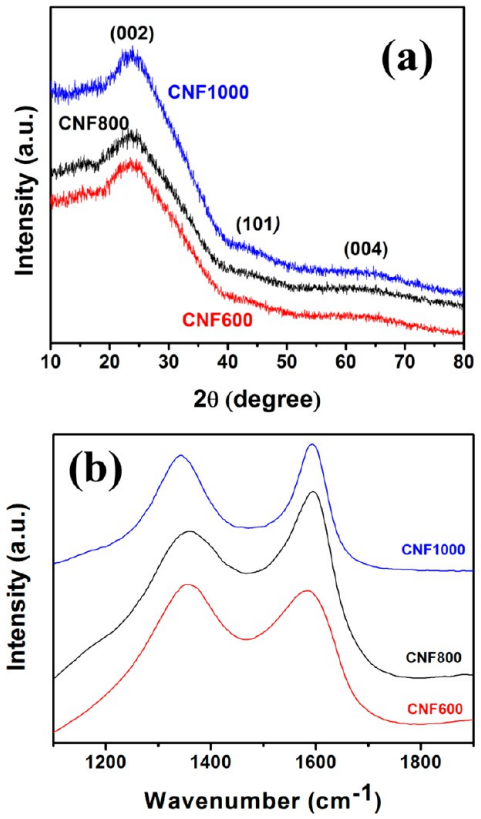

Figure 2. (a) XRD patterns and (b) Raman spectra of electrospun CNFs according to different preparation conditions.

which corresponds to the (002) *hkl* line. Secondary (101) and tertiary (004) peaks, which are also assigned to graphitic structures,[36] are very weak indicating the limited graphitization degree due to the low carbonization temperature even at a prolonged annealing process. These peaks pretend to be more prominent when the carbonization went up to 1000 °C, suggesting a higher crystallization in CNF-1000. Raman spectra provide additional evidence to confirm the partial graphitization of electrospun CNFs prepared at low temperatures (Figure 2b). For CNF-600, the peak at ~1360 cm^{-1} (D peak, assigned to disordered turbostratic carbon), which corresponds to disordered turbostratic structure, is less intense than the one for ordered graphitic structures at ~1600 cm^{-1} (G peak, assigned to graphitic carbon), whereas this trend is reversed for CNF-800 and CNF-1000. This demonstrates that more of the graphitic structures are developed when the carbonization process is conducted at a higher temperature. The ratio of I_D (intensity of D peak) to I_G (intensity of G peak) can be applied as a parameter to determine the graphitization degree (the higher the value, the lower the graphitization degree). CNF-600 presents a value of 1.049, higher than that of CNF-800 and CNF-1000, at 0.785 and 0.898, respectively. In comparison with values from another reference,[19] these values are relatively lower, which is due to the prolonged carbonization time that increased the overall graphitization. From the BET measurement, CNF-1000 has a specific surface area (SSA) of ~750 m^2 g^{-1}, while for CNF-800 and CNF-600, it decreases to ~260 and 230 m^2 g^{-1}, respectively. The average pore diameter for CNF-600, CNF-800, and CNF-1000 is 1.05, 1.88, and 2.16 nm, respectively. This demonstrates that with the increasing carbonization at a prolonged time, electrospun CNFs would

have larger contact area and slightly bigger pore ~1-2 nm in diameter. Surprisingly, the SSA of electrospun CNFs prepared at prolonged calcination time is much higher in comparison with those values of CNFs prepared at a fast heating rate and short holding time.[19] The exact reason for this difference is still under further investigation. In summary, carbonization conditions are essential to determine electrospun CNFs' structure and composition.

Electrochemical Characterization. Cyclic voltammograms (CV) of CNF-600/Li, CNF-800/Li, and CNF-1000/Li in the voltage range, 0.005−3 V, for selected cycles (1st and 5th cycle) were compared in Figure 3. In the initial discharge for

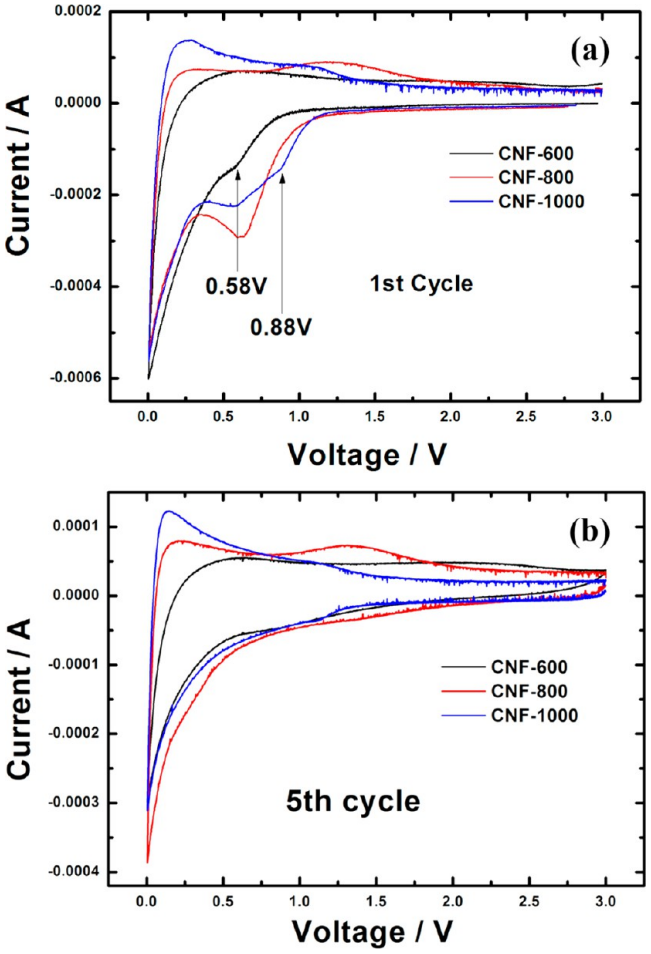

Figure 3. Cyclic voltammograms (CV) of (a) 1st discharge−charge cycle of all CNF samples and (b) 5th discharge−charge cycle of all CNF samples.

three different cells, irreversible capacity due to electrolyte decomposition and formation of solid electrolyte interphase (SEI)[37,38] could be indicated by a cathodic peak in the range from 0.58 to 0.88 V. The cathodic peak is prominent at 0.62 V for the CNF-800/Li cell, while it is less obvious at 0.58 V for the CNF-600/Li cell, which might be due to the residue hydrogen or oxygen group on CNF's surface at a low carbonization temperature. For CNF-1000, a broad peak is observed from 0.58 to 0.88 V, suggesting more than one reaction happened during the initial electrolyte decomposition on the CNF-1000 surface. Although the initial cathodic scans of electrospun CNF prepared at various carbonization temperatures are different, all demonstrate a peak with intensity variation around 0.6 V, indicating a similar electrolyte decomposition on CNFs. CNF-1000 appears to undergo other reactions assigned to the remaining part of the cathodic protuberant around 0.88 V because CNFs prepared at higher carbonization temperature pretend to have lower binding energy with lithium similar to pyrolysed hard carbon, as reported elsewhere.[39] The chemical reaction on the carbon surface during initial discharge is much more complex than formation of a single solid passivation film containing LiF, Li_2CO_3, $LiCO_2$−R, lithium alkoxides, and so forth.[37,40−42] The most prominent peak obtained by CNF-800 also coincides with the later galvanostatic profile for the largest initial irreversible capacity loss (ILC) among three cells. In the fifth cycle, the plots of cathodic scan are totally different from that of the initial cycle. No obvious peak or protuberant can be observed at a voltage higher than 0.2 V, and all electrospun CNFs demonstrate their discharge peaks close to 0 V. This further verifies the electrolyte decomposition and formation of SEI completed mostly in the initial discharge, which indicates little capacity loss in the further cycling for electrospun CNFs. Interestingly, anodic scan plots for electrospun CNFs prepared at different temperatures are also different from each other. CNF-600 presents the lowest charging plateau at higher voltage range from 0.5 to 1.0 V, whereas CNF-800 and CNF-1000 have prominent peaks below 0.3 V referring to a good deintercalation mechanism with lithium. Small voltage hysteresis is also obvious for both CNF-800 and CNF-1000 over 1.0 V, where it can be assigned to the residue hydrogen content after pyrolysis (<0.5% by mass).[43] They are supposed to be reversible and slowly degrade during cycling;[44] our result for the fifth cycle also demonstrates similar curves for 5th cycle as with the initial cycle.

Galvanostatic cycling profiles from the 1st cycle to the 500th cycle for CNF-600, CNF-800, and CNF-100 are shown in Figure 4a, b, and c, respectively. The profile of the initial cycle for CNF-600 is highly polarized due to the large quantity of residue hydrogen and the −CN group (cyano group) on the surface of the nanofibers.[35] From the long plateau ~0.419 V at the first cycle, a very large irreversible capacity (~300 mAh g^{-1}, half of the initial discharge capacity) due to electrolyte decomposition can be observed. Such high polarization trend changes when long cycling has been performed as they irreversibly trap lithium ions leading to capacity loss for the material initially. As has been reported by another reference,[19] electrospun CNFs prepared at low carbonization less than 1000 °C have some characteristics of hydrogen-contained carbons, where initial high polarization occurs and cycling capacity decays slowly. For CNF-800 and CNF-1000, the irreversible electrolyte decomposition and SEI formation are also obvious, but they occurred at a higher voltage ~0.8 V, which is similar to that of graphite.[44] This is evidence that with higher carbonization temperature electrospun CNFs evolve more graphitic structures, as verified by previous characterization. The plateau for CNF-800 is longer and more prominent than CNF-1000, thus delivering a higher capacity. As cycling number increases, the reversible capacity for three samples all moderately fade at first, which can be attributed to the remaining hydrogen weakly bound to the carbon surface. They can provide additional lithium accommodation for carbon, whereas they also slowly leave the carbon surface during cycling.[43,44] After the initial cycles for decreasing capacities, the overall charge and discharge capacities increase continuously for the next hundred cycles, especially for CNF-800 and CNF-1000. The final capacity fade

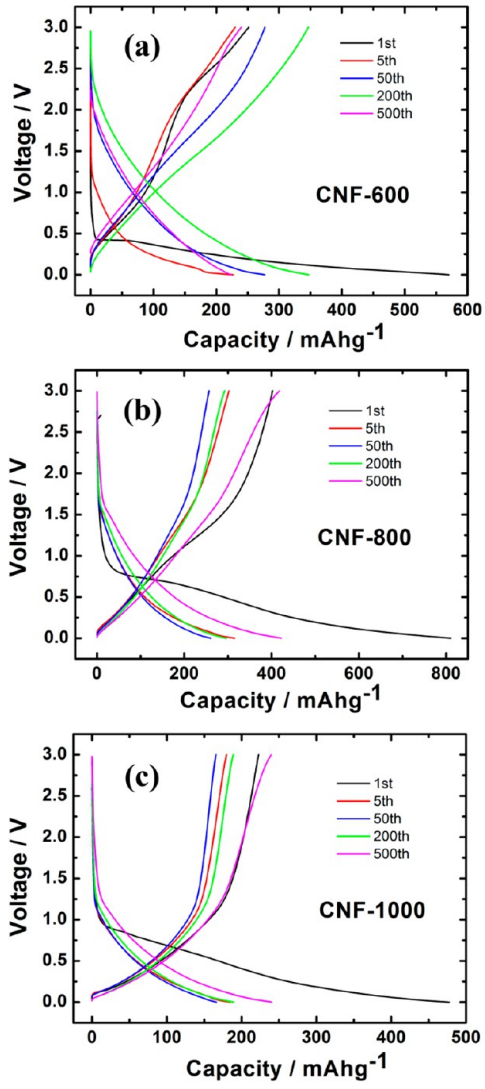

Figure 4. Galvanostatic cycling profile of (a) cell Li/CNF-600, (b) cell Li/CNF-800, and (c) cell Li/CNF-1000 at the 1st, 5th, 50th, 200th, and 500th cycle. Voltage range: 0.005−3 V; current rate: 100 mAg^{-1}.

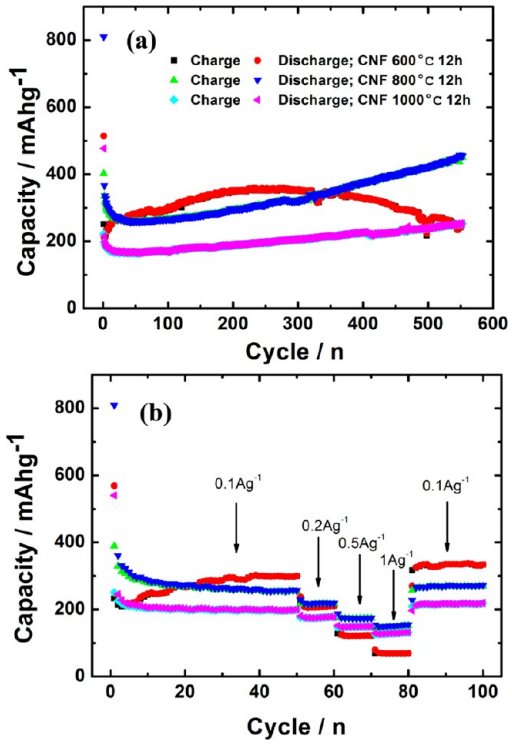

Figure 5. (a) Capacity vs cycle number plots of Li/CNF cells up to 550 cycles at a current rate of 100 mAg^{-1}. Voltage range: 0.005−3 V. (b) Rate capacity studies taken for three batches of Li/CNF cells at rates of 100, 200, 500, and 1000 mAg^{-1}.

of CNF-600 can be attributed to the cell failure after long-term cycles, which might be due to the low electronic conductivity caused by the low carbonization temperature.[29] From the cyclic profile, the curves for CNF-800 and CNF-1000 in the 200th and 500th cycles are indicating the absorbing behavior of Li ions on CNFs' surface, which can ease a higher current during cycling.[45] This coincides well with the capacity versus cycle number graphs shown in Figure 5.

More than 500 cycles for three electrospun CNFs are presented in Figure 5a, cycling at a mild current rate of 100 mAg^{-1}, which is around 0.27 C for conventional graphite. The initial columbic efficiencies for electrospun CNFs were found all below 50 % due to the high surface area reacting with electrolyte and forming SEI. The reversible capacity for CNF-800 decreases from ∼340 to ∼260 $mAhg^{-1}$ in the initial 50 cycles, and then the capacity keeps increasing to ∼460 $mAhg^{-1}$ at the end of 550th cycle. Compared with the value at the start of cycling, the total increase is ∼35%. The condition is similar to CNF-1000, but the total increase is relatively low at ∼28%, delivering a capacity ∼255 $mAhg^{-1}$ at the end of 550th cycle. For CNF-600, the material shows disturbed conductivity along the cycling process, obtaining its highest capacity of ∼360 $mAhg^{-1}$ at the 230th cycle and fading to 240 $mAhg^{-1}$ at the 550th cycle. In Figure 5b, studies on rate capacity of electrospun CNFs prepared at different temperatures are presented. CNF-800 also demonstrates the highest reversible capacity at high current rate charge−discharge at 200, 500, and 1000 mAg^{-1} (2.68 C for graphite) among all three samples, indicating a good capability of sustaining high current. At a charge−discharge rate of 2.68 C, CNF-800 can still offer a reversible capacity at ∼152.7 $mAhg^{-1}$. Comparative studies on PAN-carbonized powder at 800 °C for 12 h running at 1 Ag^{-1} verify the significance of designing 1D nanostructures for enhancing the performance (see Figure S1 in the Supporting Information). However, the decrease of capacity is less for high rate cycling with the increasing carbonization temperature, as for CNF-1000. A much greater capacity decrease at higher cycling rate is observed for CNF-600, possibly due to its poor conductivity. Reversible capacity is retained when the charge−discharge cycling carried at low, high, and again cycled at low current rate of 100 mAg^{-1} (Figure 5b). The overall capacity obtained at a mild charge−discharge rate is recovering for CNF samples at longer cycling time. Although such facts have been noted for carbonaceous materials in nanomorphology via many references,[20,46−48] the exact mechanism has not been fully understood. Similar phenomena of increasing capacity with cycle number have also been noted with many other metal oxides.[47,49−51] The high catalytic activity of metal oxide nanoparticles are believed to support the reversible formation of polymer species, which can deliver additional capacity during cycling. However, whether such mechanism is applicable to carbonaceous nanostructure is still questionable. The SEM images of cycled electrodes after long-term Li discharge/charge

up to 550 cycles are shown here to make the comparison. Figure 6a, b, and c refer to cycled electrodes of CNF-600, CNF-800, and CNF-1000, respectively. The counting histograms of fibrous diameter are also shown. Obviously, the fiber diameters increase to some extent after long-term lithiation/delithiation, but they are able to hold their fibrous morphology. After cycling, the average diameter of CNF-600 changed from 310 to 400 nm within a range of 270−560 nm. CNF-800 (210−390 nm) and CNF-1000 (230−370 nm) expand to an average value around 270 nm at a similar expansion rate of 30%. Minimal intrinsic corruption of CNF parallel to its direction was observed. This can be understood because along the CNF axis Li^+ intercalation or absorption is preferred due to the shorter diffusion path, thus preventing large stress−strain occurring parallel to CNF's direction. Therefore, the stability of electrospun CNF and its original nanofibrous morphology with partial expansion in the diameter of the fibers can be retained during long-term cycling .

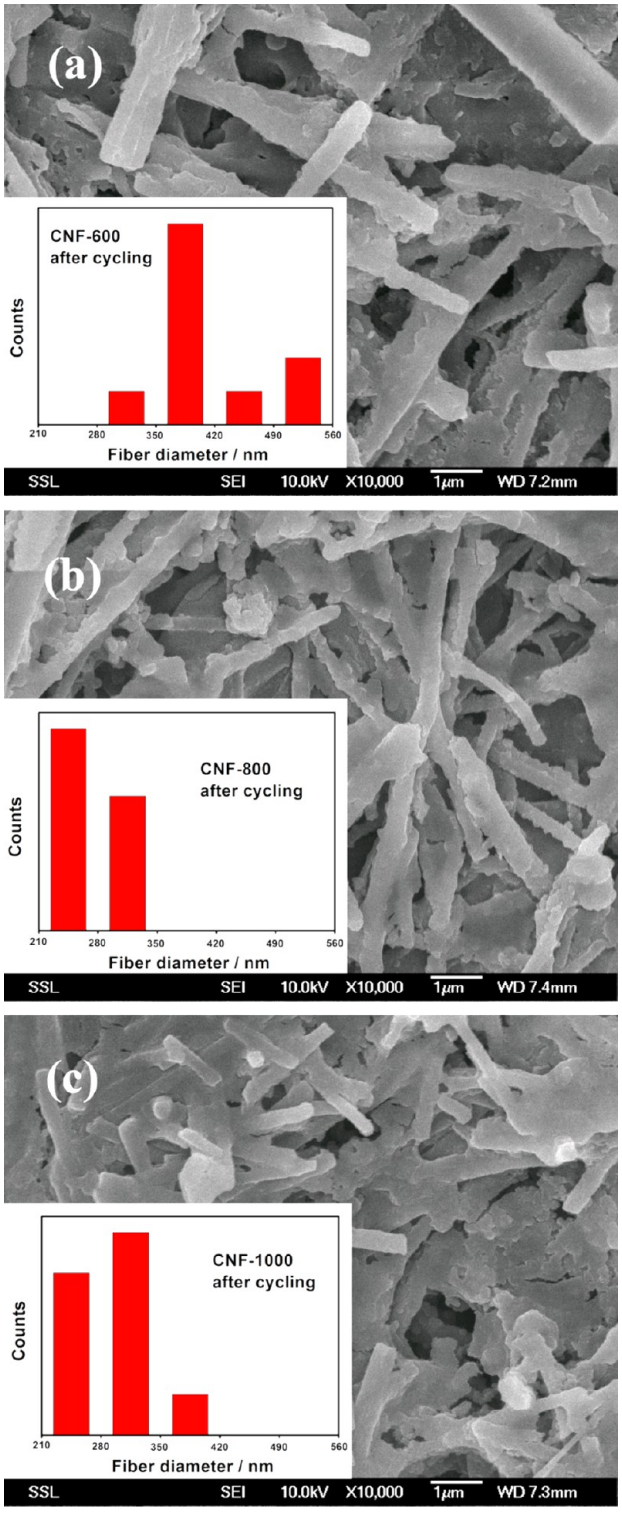

Figure 6. SEM images of cycled electrodes (after 550 cycles) with histograms of fibrous diameter: (a) for CNF-600, (b) for CNF-800, and (c) for CNF-1000.

Here, we hypothesize that the increasing capacity does have a relationship with the volumetric expansion of CNFs during long-term cycling, which is confirmed by the SEM morphology characterization above. This is possible as all nanostructured carbon materials have relatively large surface area and nanoporous characteristics so that they can contact Li ions more easily and relieve interlayer stress by volumetric expansion without deteriorating their own structures. Although it would be very difficult to calculate the extra capacity due to the complexity of many effects for the nanocarbon surface with both graphitic and turbostratic structures, the increased percentage of reversible capacity during long-term cycling is close to that of the volumetric expansion. The TEM images were taken for selected CNF-800 electrodes (Figure 7). The original CNF-800 shows a smooth surface (Figure 7b), whereas the cycled CNF-800 demonstrates volume expansion on the edge (Figure 7c). It can be indicated in the TEM images for fresh CNF-800 in Figure S2 (see the Supporting Information) that the microstructures are turbostratic carbon in the center core coated by a thin graphitic layer at the outside. Such a structure, similar to that of carbon-coated nature graphite,[52] is favorable to deliver superior electrochemical performance as an anode. After cycling, the volume of the nanofibers expands on their edges (Figure 7a,c). XRD and Raman results for cycled electrodes (see Figure S3, S4 in the Supporting Information) demonstrate minimal structural changes and no SEI residue, such as LiF or $LiCO_3$ on the CNF surface. Therefore, the observed volume expansion during cycling might be attributed to graphene layer exfoliation that might increase the contact area and greatly affect the lithium accommodation on the surface. Although exfoliation of graphite was believed to destroy the overall structure and cause capacity fading,[53] the situation would be different for carbonaceous nanostructures. As demonstrated in Figure S1 (see the Supporting Information), CNF-800 would sustain its good electrochemical cycling in comparison with directly carbonized PAN powders. The exfoliated layers on the CNF edges that appear during long-term cycling would offer additional sites for Li ions corresponding to the increasing capacity. However, the composition of the exfoliated layers needs further verification by either statistical study or experimental observation.

Electrochemical Kinetic Studies. Electrochemical kinetic studies were conducted to evaluate the Li^+ diffusion of electrospun CNFs. The galvanostatic intermittent titration technique (GITT), a reliable technique to determine the changes of the chemical diffusion of lithium (D_{Li^+}), was applied during cycling for electrospun CNFs. By applying a constant charging current flux at 100 mAg^{-1} for a limited time period τ, which is 1 h, the voltage of the cell at an equilibrium potential (E_o) would increase to a new value due to the changed amount of lithium content in electrospun CNFs. Afterwards, the cell

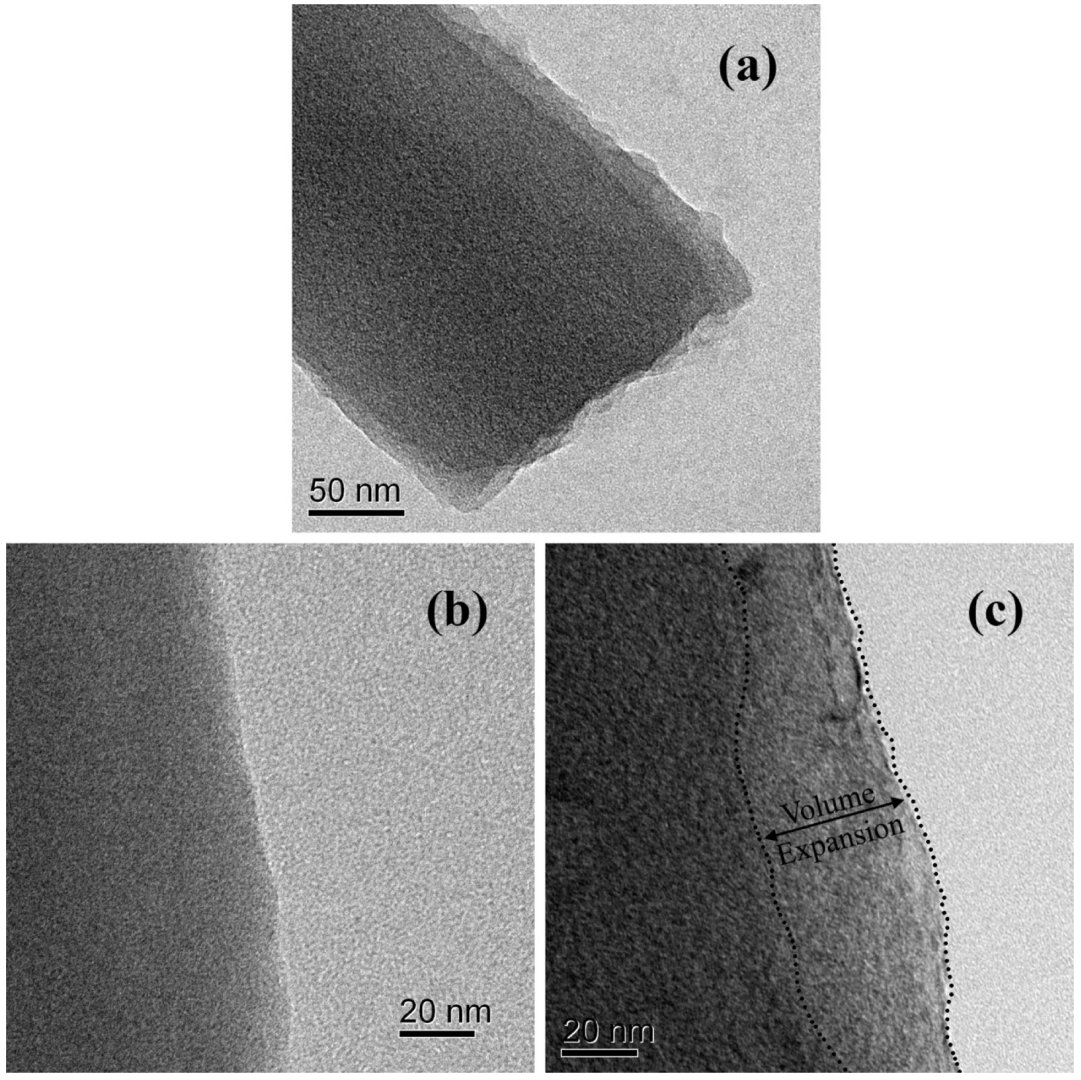

Figure 7. (a) TEM images of CNF-800 after 550 cycles in the cell. HRTEM images of (b) CNF-800 fresh samples and (c) 550-cycled CNF-800 (charged state at 3.0V).

was kept under open circuit voltage (OCV) for a duration of 5 h to reach a new steady-state potential (E_s), from which the change ΔE_s equals the difference between E_o and E_s. As shown in Figure 8a, the current flux and the resulting voltage profile for a single titration are at 0.15 V. The value of D_{Li}^+ is determined by the Fick's second law of diffusion, and the equation can be simplified as the following equation when ΔE_s for a single titration is small:[54−57]

$$D_{Li^+} = \frac{4}{\pi\tau}\left(\frac{m_B V_m}{M_B A}\right)^2\left(\frac{\Delta E_s}{\Delta E_\tau}\right)^2, (\tau \ll L^2/D_{Li^+}) \quad (1)$$

where V_m is the molar volume of the compound, M_B and m_B are molecular weight and mass, respectively, A is the total contact area between the electrolyte and electrode (geometrical area of the electrode : 2 cm^2), and L is the thickness of the electrode (electrode thickness: 10 μm). The variation of cell voltage at 0.15 V during the time period τ on application of current flux has been plotted against $\sqrt{\tau}$ in Figure 8b. The almost straight line behavior for E versus $\sqrt{\tau}$ is considered necessary for the simplification of eq 1.[54] Figure 8c demonstrates the variation of as-calculated D_{Li}^+ value when charging the CNF−Li cells from 0.005 V to 3 V. The values for CNFs prepared at different temperatures are on the same order around the similar voltage range, and they are on the order of 10^{-7} cm^2 s^{-1}, comparatively much higher than that of graphite.[38,58] The higher Li^+ diffusion rate of electrospun CNFs corresponds well with the benefits of 1D nanostructure including short diffusion path for ions.[59] At a low voltage range under 0.5 V, the Li^+ diffusion is fast, whereas the value goes down quickly afterwards as Li content becomes less in CNF. CNF-600 and CNF-800 show a more sluggish diffusion value decrease from 1.0 to 3.0 V than CNF-1000, possibly due to the residue hydrogen and nitrogen remaining at a lower carbonization temperature. With a little fluctuation around 1.5 V for CNF-600 and CNF-800, the overall trend of diffusion value is similar to the graphite. The highest D_{Li}^+ value obtained is 1.86 $\times 10^{-7}$ cm^2 s^{-1} from CNF-800 at 0.145 V, indicating a better Li^+ diffusion at phase transfer of the deintercalation process. Despite the previous finding that smaller graphite particles have a lower diffusion coefficient,[60] electrospun CNFs do not follow the same trend as they are on 1D nanoscale. The edge effects on the nanofiber surface should be reconsidered not as pronounced as micro-size graphite particles due to the exfoliated layers during cycling. On the contrary, the size effect for narrower nanofibers to have shorter diffusion pathways is more dominant in this case.

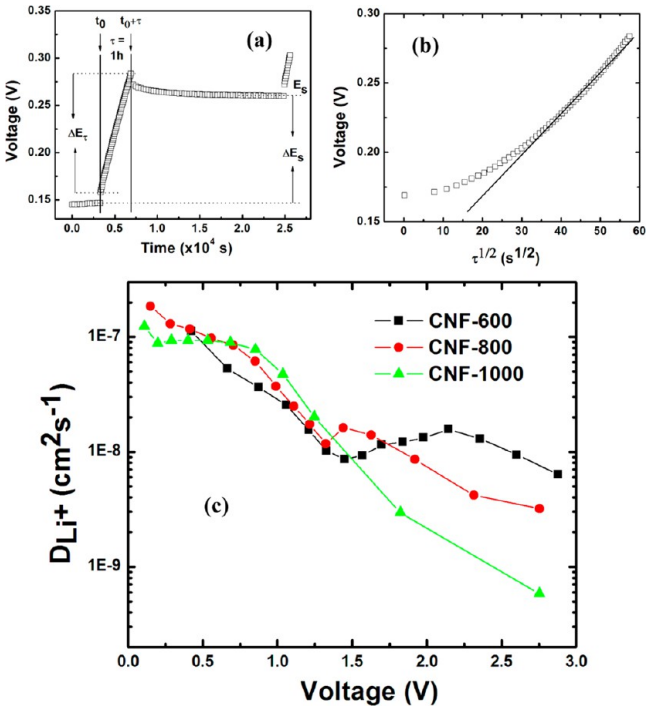

Figure 8. (a) Applied current pulse vs voltage profile for a single titration at 0.15 V during the fifth charge cycle for the CNF-800/Li cell with schematic presentation of different parameters. (b) Variation of cell voltage for the above titration plotted against $\tau^{0.5}$ to show the linear fit. (c) Variation of D_{Li}^{+} as a function of cell voltage determined by GITT during charge cycle for the CNF-600/Li, CNF-800/Li, and CNF-1000/Li cell, respectively.

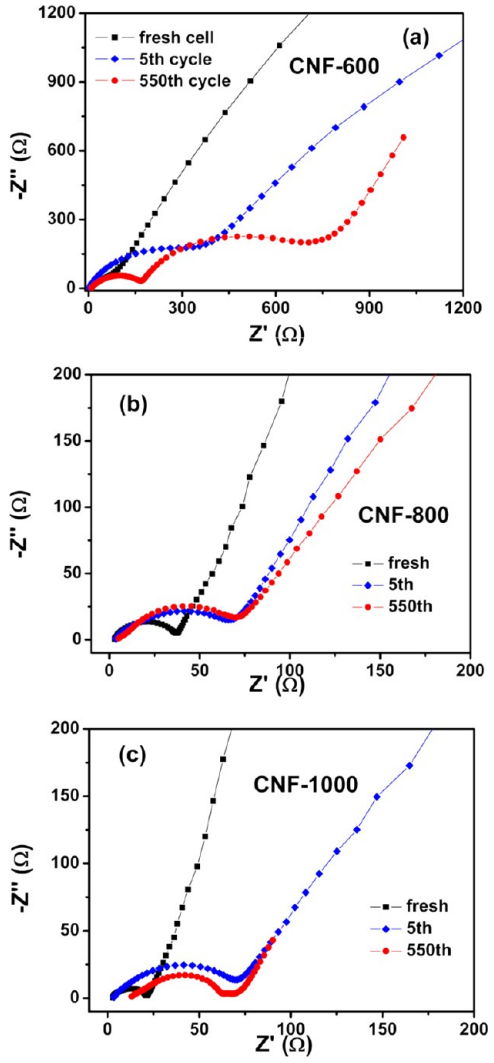

Figure 9. Family of Nyquist plots for the electrodes under different cycling conditions: fresh cells, cells after 5 cycles of discharge−charge, and cells after 550 cycles of discharge−charge. The orders are (a) CNF-600, (b) CNF-800, and (c) CNF-1000, respectively.

Figure 9 demonstrates the Nyquist plots for electrospun CNF cells. Fresh cells, 5-time cycled cells, and long-term cycled cells (the same cell after the 5th and the 550th cycling) were tested by a Solartron impedance/gain-phase analyzer. All cycled cells were tested at charged state at 3 V. Figure 9a demonstrates three different curves for CNF-600. The cell initially shows a high resistance with a large imperfect semicircle around 100 Ω, indicating the poor electrochemical property for CNF-600. The performance is correlating with its sluggish electrochemical behavior verified by GITT studies and GV profiles. After 5 cycles, the impedance value increases more than 3-fold, indicating large resistance has occurred during initial cycles. The Nyquist plots (Z′ vs Z″) after long-term cycling for 550 cycles are showing two split semicircles (Figure 5a) The first semicircle is due to a combination of surface film and charge transfer resistance, and the second semicircle is due to bulk resistance which arises due to electronic conductivity of the active material and ionic conductivity of the electrolyte.[61,62] High resistance is due to low conductivity which leads to fracture of CNF-600 cells, as indicated by Figure 5a as well. For CNF-800 and CNF-1000, both electrodes demonstrate good electric conductivity and low impedance resistance below 80 Ω with a slightly larger single semicircle than the initial one at the charged state. The initial impedance increases at the 5th cycle, and, interestingly, the semicircles for CNF-800 and CNF-1000 are not enlarged after the long-term cycling; thus, the two sample electrode could have kept good electrochemical kinetics even with volume expansion on CNFs' edges. Especially for CNF-800, the long-term cycled semicircle is similar to that of the 5th cycle Nyquist plots, which indicates well-sustained electronic contact of electrospun CNFs with the electrolyte and its good conductivity.

CONCLUSIONS

From all the results demonstrated on the long-term cycling of the electrospun CNFs as an anodic material, a better understanding of carbonaceous 1D nanostructure can be obtained through this study. Electrospun CNFs, which can be produced on large scale in the nanostructure level, were proven to have stable cycling performance and high rate capacity. CNF-800 could deliver a reversible capacity over 400 mAhg^{-1} for more than 500 cycles at 0.27C and demonstrate stable capacity at 2.68 C. The interesting capacity recovering during long-term cycling for electrospun CNFs prepared at 600 °C and 800 °C was noted and discussed in detail. It could be attributed to the possible graphene layer exfoliation during Li^+ intercalation/deintercalation. Such good electrochemical performance was further verified by kinetic studies on GITT and EIS. In summary, electrospun CNFs are among the prospective anode materials designed for high power applications and hold promise for these applications.

■ ASSOCIATED CONTENT

Supporting Information

Electrochemical comparison studies of CNF-800 and carbon derived from PAN powders, HR-TEM image of fresh CNF-800, comparison graphs of Raman spectra and XRD patterns for fresh CNF-800, and cycled CNF-800 sample. This material is available free of charge via the Internet at http://pubs.acs.org.

■ AUTHOR INFORMATION

Corresponding Author

*E-mail: phymvvr@nus.edu.sg; reddymvvr@gmail.com; msemvvr@nus.edu.sg. Fax: + 65-67776126. Tel.: + 65-65162607.

Notes

The authors declare no competing financial interest.

■ ACKNOWLEDGMENTS

Mr. Wu would like to thank the NUS Graduate School of Integrative Science and Engineering for the scholarship provided to support his PhD study.

■ REFERENCES

(1) Tarascon, J. M.; Armand, M. *Nature* **2001**, *414*, 359−367.
(2) Arico, A. S.; Bruce, P.; Scrosati, B.; Tarascon, J. M.; Van Schalkwijk, W. *Nat. Mater.* **2005**, *4*, 366−377.
(3) Armand, M.; Tarascon, J. M. *Nature* **2008**, *451*, 652−657.
(4) Reddy, M. V.; Subba Rao, G. V.; Chowdari, B. V. R. *Chem. Rev.* **2013**, *113*, 5364−5457.
(5) Takeuchi, E. S.; Quattrini, P. J.; Greatbatch, W. *Pacing Clin. Electrophysiol.* **1988**, *11*, 2035−2039.
(6) Zhu, P. N.; Wu, Y. Z.; Reddy, M. V.; Nair, A. S.; Chowdari, B. V. R.; Ramakrishna, S. *RSC Adv.* **2012**, *2*, 531−537.
(7) Hao, B.; Yan, Y.; Wang, X. B.; Chen, G. *ACS Appl. Mater. Interfaces* **2013**, *5*, 6285−6291.
(8) Lee, K. H.; Song, S. W. *ACS Appl. Mater. Interfaces* **2011**, *3*, 3697−3703.
(9) Wu, Y. Z.; Balakrishna, R.; Reddy, M. V.; Nair, A. S.; Chowdari, B. V. R.; Ramakrishna, S. *J. Alloy. Compd.* **2012**, *517*, 69−74.
(10) Shen, L. F.; Uchaker, E.; Yuan, C. Z.; Nie, P.; Zhang, M.; Zhang, X. G.; Cao, G. Z. *ACS Appl. Mater. Interfaces* **2012**, *4*, 2985−2992.
(11) Park, M. S.; Kang, Y. M.; Wang, G. X.; Dou, S. X.; Liu, H. K. *Adv. Funct. Mater.* **2008**, *18*, 455−461.
(12) Chan, C. K.; Peng, H. L.; Liu, G.; McIlwrath, K.; Zhang, X. F.; Huggins, R. A.; Cui, Y. *Nat. Nanotechnol.* **2008**, *3*, 31−35.
(13) Zhong, X.; Qu, Y. Q.; Lin, Y. C.; Liao, L.; Duan, X. F. *ACS Appl. Mater. Inter.* **2011**, *3*, 261−270.
(14) Wu, Y. Z.; Chowdari, B. V. R.; Ramakrishna, S. *Curr. Org. Chem.* **2013**, *17*, 1411−1423.
(15) Agend, F.; Naderi, N.; Fareghi-Alamdari, R. *J. Appl. Polym. Sci.* **2007**, *106*, 255−259.
(16) Kim, C.; Yang, K. S.; Kojima, M.; Yoshida, K.; Kim, Y. J.; Kim, Y. A.; Endo, M. *Adv. Funct. Mater.* **2006**, *16*, 2393−2397.
(17) Bonino, C. A.; Ji, L. W.; Lin, Z.; Toprakci, O.; Zhang, X. W.; Khan, S. A. *ACS Appl. Mater. Interfaces* **2011**, *3*, 2534−2542.
(18) Inagaki, M.; Yang, Y.; Kang, F. Y. *Adv. Mater.* **2012**, *24*, 2547−2566.
(19) Lee, B. S.; Son, S. B.; Park, K. M.; Yu, W. R.; Oh, K. H.; Lee, S. H. *J. Power Sources* **2012**, *199*, 53−60.
(20) Qie, L.; Chen, W. M.; Wang, Z. H.; Shao, Q. G.; Li, X.; Yuan, L. X.; Hu, X. L.; Zhang, W. X.; Huang, Y. H. *Adv. Mater.* **2012**, *24*, 2047−2050.
(21) Huang, Z. M.; Zhang, Y. Z.; Kotaki, M.; Ramakrishna, S. *Compos. Sci. Technol.* **2003**, *63*, 2223−2253.
(22) Li, D.; Babel, A.; Jenekhe, S. A.; Xia, Y. N. *Adv. Mater.* **2004**, *16*, 2062−2066.
(23) Cherian, C. T.; Sundaramurthy, J.; Reddy, M. V.; Kumar, P. S.; Kalaivani, M.; Pliszka, D.; Sow, C. H.; Ramakrishna, S.; Chowdari, B. V. R. *ACS Appl. Mater. Interfaces* **2013**, *5*, 9957−9963.
(24) Zhang, L. F.; Hsieh, Y. L. *Eur. Polym. J.* **2009**, *45*, 47−56.
(25) Bahl, O.; Shen, Z.; Lavin, J.; Ross, R. *Carbon Fibers*, 3rd ed.; Marcel Dekker: New York, 1998; pp 1−83.
(26) Niu, H. T.; Zhang, J.; Xie, Z. L.; Wang, X. G.; Lin, T. *Carbon* **2011**, *49*, 2380−2388.
(27) Ji, L. W.; Zhang, X. W. *Electrochem. Commun.* **2009**, *11*, 1146−1149.
(28) Ji, L. W.; Lin, Z.; Guo, B. K.; Medford, A. J.; Zhang, X. W. *Chem.—Eur. J.* **2010**, *16*, 11543−11548.
(29) Wang, Y.; Santiago-Aviles, J. J.; Furlan, R.; Ramos, I. *IEEE Trans. Nanotechnol.* **2003**, *2*, 39−43.
(30) Wu, Y. Z.; Balakrishna, R.; Reddy, M. V.; Nair, A. S.; Chowdari, B. V. R.; Ramakrishna, S. *J. Alloy. Compd.* **2012**, *517*, 69−74.
(31) Wu, Y. Z.; Zhu, P. N.; Zhao, X.; Reddy, M. V.; Peng, S. J.; Chowdari, B. V. R.; Ramakrishna, S. *J. Mater. Chem. A* **2013**, *1*, 852−859.
(32) Jing, M.; Wang, C. G.; Wang, Q.; Bai, Y. J.; Zhu, B. *Polym. Degrad. Stab.* **2007**, *92*, 1737−1742.
(33) Liu, J.; Wang, P. H.; Li, R. Y. *J. Appl. Polym. Sci.* **1994**, *52*, 945−950.
(34) Zhang, W. X.; Liu, J.; Wu, G. *Carbon* **2003**, *41*, 2805−2812.
(35) Yusof, N.; Ismail, A. F. *J. Anal. Appl. Pyrolysis* **2012**, *93*, 1−13.
(36) Mittal, J.; Bahl, O. P.; Mathur, R. B. *Carbon* **1997**, *35*, 1196−1197.
(37) Fong, R.; Vonsacken, U.; Dahn, J. R. *J. Electrochem. Soc.* **1990**, *137*, 2009−2013.
(38) Verma, P.; Maire, P.; Novak, P. *Electrochim. Acta* **2010**, *55*, 6332−6341.
(39) Buiel, E.; Dahn, J. R. *Electrochim. Acta* **1999**, *45*, 121−130.
(40) Aurbach, D.; Zaban, A. *J. Electroanal. Chem.* **1993**, *348*, 155−179.
(41) Kanamura, K.; Tamura, H.; Shiraishi, S.; Takehara, Z. *J. Electroanal. Chem.* **1995**, *394*, 49−62.
(42) Peled, E.; Golodnitsky, D.; Ardel, G. *J. Electrochem. Soc.* **1997**, *144*, L208−L210.
(43) Zheng, T.; McKinnon, W. R.; Dahn, J. R. *J. Electrochem. Soc.* **1996**, *143*, 2137−2145.
(44) Dahn, J. R.; Zheng, T.; Liu, Y. H.; Xue, J. S. *Science* **1995**, *270*, 590−593.
(45) Kumar, P. S.; Sahay, R.; Aravindan, V.; Sundaramurthy, J.; Ling, W. C.; Thavasi, V.; Mhaisalkar, S. G.; Madhavi, S.; Ramakrishna, S. *J. Phys. D: Appl. Phys.* **2012**, *45*, 509901.
(46) Yang, S. B.; Feng, X. L.; Zhi, L. J.; Cao, Q. A.; Maier, J.; Mullen, K. *Adv. Mater.* **2010**, *22*, 838−842.
(47) Xu, Y. H.; Guo, J. C.; Wang, C. S. *J. Mater. Chem.* **2012**, *22*, 9562−9567.
(48) Magasinski, A.; Dixon, P.; Hertzberg, B.; Kvit, A.; Ayala, J.; Yushin, G. *Nat. Mater.* **2010**, *9*, 353−358.
(49) Guo, B. K.; Shu, J.; Tang, K.; Bai, Y.; Wang, Z. X.; Chen, L. Q. *J. Power Sources* **2008**, *177*, 205−210.
(50) Laruelle, S.; Grugeon, S.; Poizot, P.; Dolle, M.; Dupont, L.; Tarascon, J. M. *J. Electrochem. Soc.* **2002**, *149*, A627−A634.
(51) Debart, A.; Dupont, L.; Poizot, P.; Leriche, J. B.; Tarascon, J. M. *J. Electrochem. Soc.* **2001**, *148*, A1266−A1274.
(52) Yoshio, M.; Wang, H. Y.; Fukuda, K.; Hara, Y.; Adachi, Y. *J. Electrochem. Soc.* **2000**, *147*, 1245−1250.
(53) Chung, G. C.; Kim, H. J.; Yu, S. I.; Jun, S. H.; Choi, J. W.; Kim, M. H. *J. Electrochem. Soc.* **2000**, *147*, 4391−4398.
(54) Shaju, K. M.; Subba Rao, G. V.; Chowdari, B. V. R. *Electrochim. Acta* **2003**, *48*, 2691−2703.
(55) Shaju, K. M.; Subba Rao, G. V.; Chowdari, B. V. R. *J. Electrochem. Soc.* **2003**, *150*, A1−A13.
(56) Shaju, K. M.; Subba Rao, G. V. ; Chowdari, B. V. R. *J. Mater. Chem.* **2003**, *13*, 106−113.

(57) Reddy, M. V.; Jose, R.; Viet, A. L.; Ozoemena, K. I.; Chowdari, B. V. R.; Ramakrishna, S. *Electrochim. Acta* **2013**, DOI: 10.1016/j.electacta.2013.10.003.
(58) Markevich, E.; Levi, M. D.; Aurbach, D. *J. Electroanal. Chem.* **2005**, *580*, 231−237.
(59) Mai, L. Q.; Xu, L.; Han, C. H.; Xu, X.; Luo, Y. Z.; Zhao, S. Y.; Zhao, Y. L. *Nano Lett.* **2010**, *10*, 4750−4755.
(60) Markovsky, B.; Levi, M. D.; Aurbach, D. *Electrochim. Acta* **1998**, *43*, 2287−2304.
(61) Reddy, M. V.; Subba Rao, G. V.; Chowdari, B. V. R. *J. Mater. Chem.* **2011**, *21*, 10003−10011.
(62) Reddy, M. V.; Wen, B. L. W.; Loh, K. P.; Chowdari, B. V. R. *ACS Appl. Mater. Interfaces* **2013**, *5*, 7777−7785.